ACS OMEGA

http://pubs.acs.org/journal/acsodf

Article

Influence of Fish Scale-Based Hydroxyapatite on Forcespun Polycaprolactone Fiber Scaffolds

Deepa Kodali, Vincent Hembrick-Holloman, Dilip Reddy Gunturu, Temesgen Samuel, Shaik Jeelani, and Vijaya K. Rangari*

Cite This: *ACS Omega* 2022, 7, 8323−8335

Read Online

ACCESS | Metrics & More | Article Recommendations

ABSTRACT: Marine waste byproducts, especially fish scales, have proved to be one of the most prominent sources for developing sustainable materials for various applications including biomedical applications. Hydroxyapatite (HAp), being one of such biomaterials that can be synthesized from the massive fish-based waste, has received plentitude of attention due to its excellent ability to promote cell growth and proliferation. However, understanding the influence of HAp on polymer matrices that are tailored for biomedical applications is still a challenge. This study is intended to develop a sophisticated yet inexpensive method to obtain nonwoven polycaprolactone (PCL) nanofibrous scaffolds and analyze the influence of calcium-deficient nanoporous hydroxyapatite (n-HAp) on the thermal, mechanical, and biological properties of these scaffolds. The n-HAp is synthesized using two different types of fish scales, carpa (CA) and pink perch (PP), by calcination followed by nanomilling. The synthesized n-HAp powder is characterized by using X-ray diffraction, scanning electron microscopy (SEM), transmission electron microscopy (TEM), and X-ray photoelectron spectroscopy. The PCL fibrous scaffolds were developed using a novel forcespinning technique with n-HAp as the filler. The morphology of the scaffolds was characterized using SEM and Raman spectroscopy. SEM and TEM results have confirmed the size reduction of the HAp powder after nanomilling. Thermal properties were analyzed using thermogravimetric analysis and differential scanning calorimetry. The major degradation temperature has increased by 3° and was observed to be 398° for 1 wt % filler loading for both carpa and pink perch-derived n-HAp. The increase in filler content has increased the residue left after decomposition and is 4% for 5 wt % filler loading. The crystallinity percent has increased by 7% compared to neat fibers for 1 wt % filler loading. Mechanical properties were tested using tensile tests. The tensile test strength has shown 32% improvement for 1 wt % compared to neat fibers. Cell viability tests were performed using hFOB cells which have shown significant cell growth for a high filler loading of 5 wt %. The results suggest that both CA-n-HAP and PP-n-Hap-incorporated fibrous scaffolds can be used potentially for biomedical applications after careful investigation of the scaffold behavior with longer incubation periods.

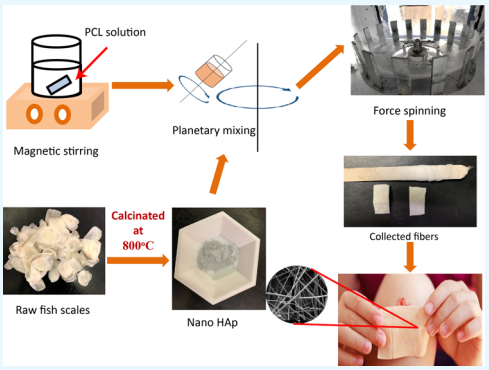

1. INTRODUCTION

In the recent years, huge demand for the sustainable materials persists and thus increased the utilization of natural resources globally which has reached 92.1 billion tons in 2017 from that of 27 billion in 1970.[1,2] Especially, the per capita consumption of fish products has perceivable progression of 20.5 kg in 2018 with an increase of 1.5 percent per year since 1961.[3] However, more than 27% of fish produced is disposed as redundant waste after processing which includes 18−30 million tons of skin, scales, fins, bones, and so forth, which results in environmental haphazards such as high chemical oxygen demands, pathogenic microbial development, and so on.[4−7] Among that, fish scales constitute of 8 million tons of waste and thus became the focus of the researchers to excogitate the ways to salvage the material.[6] Collagen, hydroxyapatite (HAp), and hydroxyproline are the prime constituents of fish scales which are used in cosmetic and biomedical applications.[8,9] The HAp derived from the fish scales is spherical, biocompatible, and bioactive.[10]

Hydroxyapatite $[Ca_{10}(PO_4)_6(OH)_2]$ belongs to a group of calcium phosphates with a Ca/P molar ratio of 1.67 and has similar chemical composition as that of the minerals present in bone and teeth enamel.[11,12] Thus, the bioceramic HAp became an ideal material for biomedical applications such as coatings, tissue engineering, scaffolds, biogenic catalysis, orthopedics,

Received: October 7, 2021
Accepted: January 5, 2022
Published: February 28, 2022

https://doi.org/10.1021/acsomega.1c05593
ACS Omega 2022, 7, 8323−8335

and odontology for repairs and regenerations.[4,12] Especially, for the material to be quintessential for scaffolds, it should have biocompatibility, porous morphology, adequate mechanical properties, biodegradability, and appropriate surface chemistry for cell proliferation.[13] HAp exhibits remarkable bioactivity, osteoconductivity, and biocompatibility in addition to being nontoxic and noninflammatory and thus serves as an excellent material for scaffolds, promoting cell colonization and reformation.[14−16]

Recently, attempts have been made to develop novel bio HAp-based scaffolds for biomedical applications. The HAp synthesized from *Labeo rohita* fish scales is used to develop Polyethyleneglycol-HAp composite porous bone scaffold from the solvent casting technique.[17] These scaffolds have exhibited interconnected porosity and satisfactory mechanical performance with a compressive strength of 4.93 Mpa, making them suitable for tissue engineering applications. The HAp from *Puntius conchonius* fish scales was used to develop poly methyl methacrylate-HAp scaffolds which can be used for segmental bone defect treatment. Furthermore, the in vitro bioactivity analysis studies of these scaffolds have confirmed the presence of apatite that is similar to bone on the scaffold surface.[18] The salmon and red snapper fish scale-based HAp is used to develop novel peptide-based hybrid scaffolds for periodontal applications which showed promising properties.[19] While the salmon-based HAp has shown remarkable mechanical properties, snapper-based HAp has exhibited greater alignment of cells. The poly(lactide-*co*-glycolide) fibrous membrane infused with fish-based collagen and chemically synthesized HAp was developed from the electrospinning method for guided bone regeneration. Thus, developed membranes have attained the standards of biological evaluation of medical devices and thus have proven that they were highly suitable for tissue regeneration.[20,21] Nano crystalline HAp is synthesized from *Catla catla* fish scales by calcination and is sintered to evaluate the bioactivity by culturing it with human osteoblast-like cells and mouse osteoblast cell line which proved that synthesized HAp is nontoxic.[8] The fish scale powder obtained from *Acanthopagrus schlegelii* is high in HAp and is utilized to develop polyhydroxyalkanoate composite nanofibers via electrospinning for biomedical applications. The hydrophilic effect due to the presence of fish scale powder has provided a convenient environment for the growth of cells.[9] The fish bone extract has proved to improve cell proliferation along with calcium deposition when coated on 3D-printed polycaprolactone (PCL) scaffolds.[22] Fish scale-based mineral-ion HAp-loaded poly lactic acid (PLA)/chitosan composite scaffolds were developed by an in situ blending technique. These scaffolds have shown improved cell adhesion and alkaline phosphate activity in addition to the desired compressive strength which is suitable for tissue engineering applications.[23] The fish scale-derived HA has improved corrosion performance and biomineralization of the magnesium-based implants.[24,25]

Although efforts were made to effectively utilize the HAp synthesized from fish scales, there is still existing demand for the bio-based HAp composites because of their superior osteogenic properties.[18] One of the main challenges in designing the scaffolds that are suitable for bone tissue engineering is that the scaffolds should be both biocompatible and osteogenic.[26,27] In addition to the osteogenic properties, the scaffolds should have a porous structure consistent with that of host for the successful transmission of oxygen and other nutrients and also for blood vessel formation and also should possess adequate mechanical properties that match with the bone properties.[27] In general the scaffolds are fabricated from natural or synthetic polymers with bioactive materials which are biodegradable. For instance, the addition of strontium containing HAp to PCL has showed improved bioactivity with increased degradation rate. Among the polymers, PCL has become an irrefutable source for biomedical applications with suitable mechanical strength and excellent biocompatibility and biodegradability.[28,29] The semicrystalline and nontoxic nature of this aliphatic polyester makes it highly suitable for the fabrication of scaffolds for tissue engineering, drug-delivery, sutures, and bone repairs.[16] Owing to the tailored physio-mechanical and biological properties, there is a huge demand for the bioresorbable polymers such as PCL composite scaffolds with bioactive materials in tissue engineering in recent years.[30]

Despite the efforts made in developing the scaffolds in tissue engineering, the thermomechanical and biological properties are yet to be explored for various combinations of polymer matrices for the efficient use of fish scale-derived HAp. In consideration of the aforementioned limitations, in this work, we made an attempt to develop a low-cost novel method to develop PCL scaffolds infused with fish scale-derived nano HAp. We have developed PCL fibrous scaffolds infused with HAp synthesized from two types of fish scales, fresh water carpa (*Labeo catla*) and deep sea pink perch (*Nemipterus Japonicus*) scales by using a novel forcespinning technique. The forcespinning technique uses centrifugal forces to generate fibers successfully from various polymers.[31−33] While the majority of the nanofibrous scaffolds reported in the literature were generated by electrospinning method,[26] the properties of PCL scaffolds with fish scale-derived HAp from forcespinning technique have not been reported in the literature to the best of our knowledge. In this study, the thermomechanical and biological properties of the developed PCL-n-HAp scaffolds are analyzed in detail to understand the influence of fish scale derived n-HAp on the polymer composite scaffolds developed via forcespinning.

2. MATERIALS AND METHODS

2.1. Materials. The powdered PCL (molecular weight of 50000) was used to develop forcespun composite fibers and this was purchased from Polysciences, Inc (Warrington, PA, USA). Chloroform with ACS reagent ≥99.8% and tetrahydrofuran (THF) with ACS reagent ≥99% were used as solvents to dissolve PCL and were purchased from Sigma-Aldrich (St. Louis, MO, USA).

The raw fish scales of pink perch (PP) and carpa (CA) were procured from Nizona Inc., Mumbai, India. These scales were cleaned, sundried, and had a moisture content of 20−30% prior to purchasing. The scales were calcined in a box furnace at 800 °C for 3 h. The calcinated scales were then ground into a fine powder using mortar and pestle. This powder is further nanomilled for 1 h at 2000 rpm by using MTI compact nanoagitator bead mill which consists of 0.3 mm zirconia balls for the milling process with distilled water as the solvent. The nanomilled powder was then collected and then centrifuged using a Beckman coulter Allegra X-30 R centrifuge to separate n-HAp particles. Thus, the collected n-HAp powder was dried, ground again with mortar and pestle, and was labeled for use.

2.2. Forcespinning of Fibers. The powdered PCL of 16 wt % was dissolved in THF and chloroform with 70:30 (wt/

https://doi.org/10.1021/acsomega.1c05593
ACS Omega 2022, 7, 8323−8335

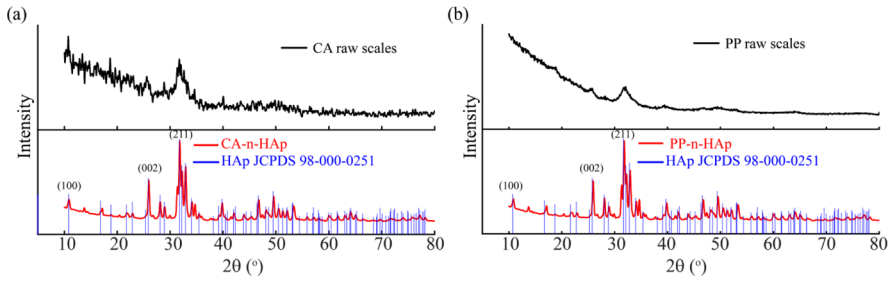

Figure 1. XRD diffractograms of raw scales and synthesized n-HAp powder of (a) carpa (CA-n-HAp) and (b) pink perch (PP-n-HAp).

wt) concentration. The PCL solution was then mixed using a magnetic stirrer for 3 h at 170 rpm for homogeneous solution. The vials were sealed during the mixing process to prevent the evaporation of solvent. The n-HAp powder from PP and CA scales was infused into the PCL solution by 1, 3, and 5 wt %. The solution was then mixed thoroughly for 7 min at 1900 rpm using a planetary noncontact Thinky mixer, ARE-250 for homogeneous dispersion.

Forcespinning Cyclone L-1000M apparatus from Fiberio equipped with solution spinneret with "24ga × 1/2" stainless steel regular bevel needle was used to obtain the nonwoven fibrous mats from the polymer solution mixture. A 2 mL precursor (PCL-n-HAp) solution was injected into the spinneret using a pipette. The angular velocity of the spinneret was maintained at 6000 rpm with a spin time of 10 min. The fibers were collected on the collector with equally spaced vertical plates placed at a distance of 115 mm from the needle (190 mm from the center of the spinneret). The detailed description of the setup can be found in the studies by Kodali et al.[34,35] Thus, the collected fibers were stored under desiccation for further characterization.

2.3. Fiber Characterization. *2.3.1. X-ray Diffraction.* The raw and calcined fish scales were analyzed using X-ray diffraction (XRD) studies using a Bruker D8 diffractometer which is equipped with monochromatic Cu Kα radiation. This was operated at a scan rate of 1°/min, with a step size of 0.02°, varying from 10 to 90° Bragg's angle of diffraction at 45 kV and 40 mA.

2.3.2. Scanning Electron Microscopy. The synthesized n-HAp particles and the morphology of the PCL-n-HAp fibers obtained were analyzed using a JEOL JSM-7200F field emission scanning electron microscope (JEOL USA, Peabody, MA) at 2 kV. The samples were sputter-coated with gold/palladium (Au/Pd) for 3 min at 10 mA using Hummer sputter coater.

2.3.3. Transmission Electron Microscopy. A JEOL 2010 transmission electron microscope was used to analyze the particle size, shape, crystallinity, and distribution of the n-HAp powder. The nanopowder was first dispersed in ethanol and then placed on the Cu grid and air dried for further transmission electron microscopy (TEM) analysis. An operating voltage of 200 kV is used for the process.

2.3.4. XPS. A VersaProbe 5000 X-ray Photoelectron Spectroscopy (XPS) instrument from Phi Electronics Inc. is used to perform surface analysis of the synthesized n-HAp powder from CA and PP scales. This instrument is equipped with a monochromatic X-ray source at 4.4 W with a spot size of 20 μm. The peak positions were not corrected as the system offers dual neutralization. The survey scans were performed at a pass energy of 187.85 eV and with a step size of 0.8 eV. The photodetector takeoff angle, which is the angle between surface normal and the axis of the analyzer lens, is considered as 45° and was used to acquire the data.

2.3.5. Raman Spectroscopy. Thermo-scientific DXR Raman spectrometer was used to carry out the Raman analysis of the fabricated PCL-n-HAp fibrous scaffolds. The laser with the excitation wavelength of 785 nm was used for the analysis. The fiber mats were placed on the glass slide and were focused by the laser beam prior to acquiring the spectrum. The spectra were obtained for a small area and were averaged for further understanding. The spectrum was analyzed in the range of 0−2000 cm^{-1} with a laser power of 5 mW.

2.3.6. Thermogravimetric Analysis. Thermogravimetric analysis (TGA) was performed using a TA Q500 Thermogravimetric Analyzer. The decomposition temperatures, weight change, and the residue left are evaluated from the weight change of the specimens with the increase in temperature. Approximately 15 mg of sample was placed on the platinum pan and heated at a rate of 10 °C/min from 30 to 800 °C for the analysis under a nitrogen atmosphere.

2.3.7. Differential Scanning Calorimetry. The thermal properties of the fibers were analyzed using differential scanning calorimetry (DSC) TA-Q series 2000. The samples weighing 10 to 12 mg approximately were sealed using hermetic pans. The DSC thermograms were obtained at a rate of 5 °C/min from −80 to 80 °C, followed by cooling to −80 °C and then heating up to 80 °C under a nitrogen flow.

2.3.8. Tensile Testing. The uniaxial tensile tests were performed to analyze the mechanical properties of the nonwoven fibrous mats with 5 mm width and 20 mm length following ASTM D882-10 standard.[36] The test window frame with fiber mat is shown in Figure 2a. The thickness was measured with a micrometer (Mitutoyo 293-340-30 digital micrometer) with 0.001 mm resolution. To obtain statistically reliable results, the average thickness of the fibrous mats was obtained by taking measurements at 10 different places.

Finally, the test window frame was placed between the grips of a Zwick/Roell Z2.5 universal mechanical testing machine, and the frame portion was cut. Displacement control mode with a constant crosshead speed of 5 mm/min, a preload of 0.01 N, and a 20 N load cell was used to perform the tensile tests. Zwick/Roell software associated with the machine calculates the slope of each stress−strain curve in its elastic deformation region to obtain the Young's modulus. Additionally, the software also gives other desired test results such as elongation at break, tensile strength, and elongation at maximum stress.

2.3.9. Cell Adhesion. To determine the adaptability of the developed nonwoven fibrous scaffolds for cell adhesion and proliferation, human Osteoblast cells (hFOB) from American Type Culture Collection (#CRL-11372) were obtained. hFOB's cells were cultivated in Dulbecco's modified Eagle

https://doi.org/10.1021/acsomega.1c05593
ACS Omega 2022, 7, 8323−8335

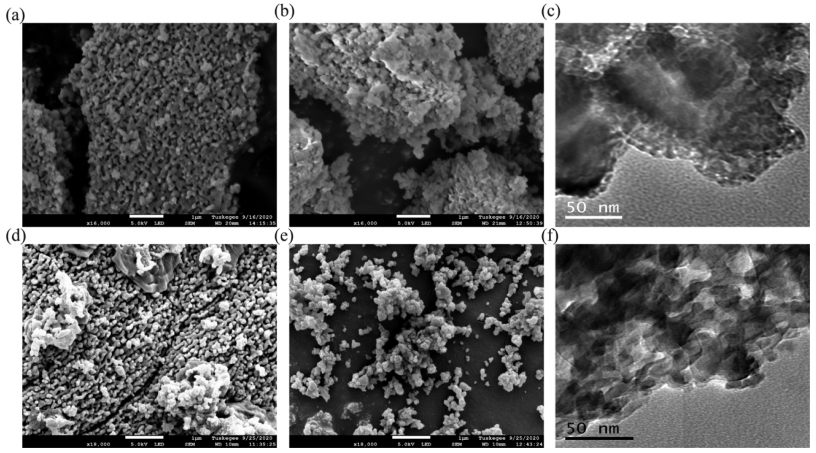

Figure 2. Morphology of synthesized n-HAp: SEM micrographs of (a) as-synthesized CA-n-Hap and (b) nanomilled CA-n-Hap and (c) TEM image of CA-n-HAp after nanomilling, SEM micrographs of (d) as-synthesized PP-n-HAp and (e) nanomilled PP-n-Hap and (f) TEM image of PP-n-HAp after nanomilling.

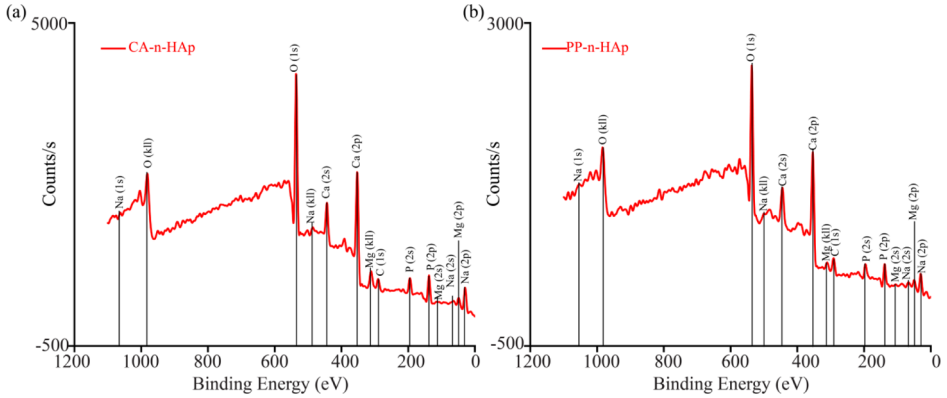

Figure 3. XPS of PCL-n-HAp fibers with (a) CA-n-HAp and (b) PP-n-HAp.

medium—high glucose containing 1% (v/v) bovine serum (FBS), L-glutamine, and 10 μg/mL ciprofloxacin (antibacterial). Cells were incubated in a humidified incubator under normal cell culture conditions (37 °C, 5% CO_2/95% air environment). The PCL scaffolds with CA and PP n-HAp with 1, 3, and 5 wt % along with neat scaffolds were seeded with hFOB cells and observed at different time intervals. The scaffolds were first sterilized in 70% ethanol for 30 min and then washed with PBS three times before seeding the cells. The seeded scaffolds were incubated for different time frames, 3 and 5 days, under normal cell culture conditions. Cell adhesion and spreading of cells were examined under a field emission scanning electron microscope. The cell-seeded scaffold samples were dehydrated, vacuum-dried, and gold/palladium coated prior to scanning electron microscopy (SEM) analysis.

3. RESULTS

3.1. Characterization of n-HAp Powder. *3.1.1. XRD of n-HAp Powder.* The XRD analyses of the CA and PP raw fish scales embodied with organic matter such as fats, proteins, collagen, and other minerals are shown in Figure 1a,b. Due to the presence of organic matter, the n-HAp peaks are not distinct in the spectrum for raw fish scales. The calcination process retains the calcium phosphate and its mineral forms while removing the organic portion.[37] The calcined and nanomilled powder from carpa (CA-n-HAp) and pink perch (PP-n-HAp) were analyzed from Figure 1a,b. The analyses show evident peaks for n-HAp that are closely matched with standard HAp (JCPDS-Pdf # 98-000-0251) and its corresponding polycrystalline hexagonal lattice cells.[35] The characteristic peaks of n-HAp powder were observed at 2θ of 25.98 and 31.83° for CA-n-HAp and 25.93 and 31.81° for PP-n-HAp which corresponds to (0,0,2) and (2,1,1) planes, respectively. Although the highest intensity for both the n-HAp powders was found for (2,1,1), the PP-n-HAp shows a relatively higher intensity compared to CA-n-HAp which suggests that the crystal growth was promoted along the *c*-axis.[38,39] Furthermore, traces of tricalcium bis(orthophosphate) was found in both the n-HAp powders (CA-n-HAp 7% and PP-n-HAp 17%) in addition to the apatite.

The crystallite sizes of the CA-n-HAp and PP-n-HAp powders were calculated from the Debye−Scherrer equation: $D = K\lambda/\beta$ Cos θ, where D is crystallite size in nm, K is the Scherrer constant and is considered as 0.94, λ is the diffraction wavelength 1.54 A°, θ is the diffraction angle, and β is the full width half maxima of the considered peak. The average crystallite size is determined by considering the average of the crystallite sizes obtained at distinct peaks in the spectrum. Thus, considered average crystallite sizes were observed to be 30.77 nm for CA-n-HAp and 30.63 nm for PP-n-Hap, which suggests that the powder obtained is in the nano range. The crystallite size of the n-HAp powder is observed to be around 10 nm at highest intensity peaks for both the scales.

https://doi.org/10.1021/acsomega.1c05593
ACS Omega 2022, 7, 8323−8335

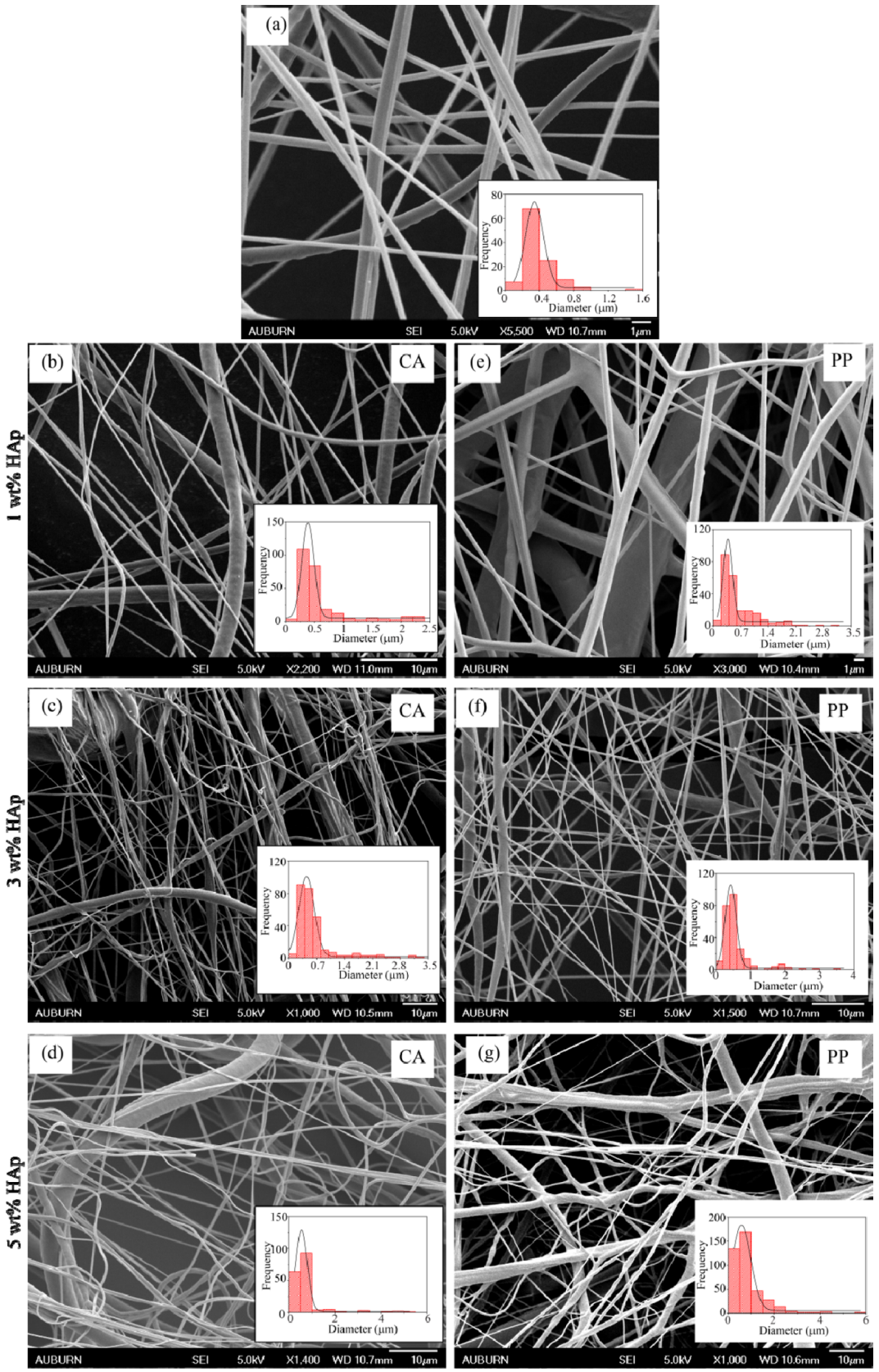

Figure 4. SEM micrographs of PCL-n-HAp fibers with corresponding histograms showing fiber diameter distribution for (a) neat, (b) CA-n-HAp 1 wt %, (c) CA-n-HAp 3 wt %, (d) CA-n-HAp 5 wt %, (e) PP-n-HAp 1 wt %, (f) PP-n-HAp 3 wt %, and (g) PP-n-HAp 5 wt %.

3.1.2. Microscopy of n-HAp Powder. The particles of the n-HAp powder that is obtained after calcination as well as after nanomilling are irregular in size and distribution as observed from the SEM micrographs shown in Figure 2. The

https://doi.org/10.1021/acsomega.1c05593
ACS Omega 2022, 7, 8323−8335

morphology of CA-n-HAp before and after nanomilling is shown in Figure 2a,b, respectively, and PP-n-HAp is shown in Figure 2d,e. The TEM micrographs of CA-n-HAp and PP-n-HAp are shown in Figure 2c,f, respectively. The n-HAp particles were observed to be agglomerated in both the cases. The synthesized powder was reduced to the nano range and was observed to be porous which is evident from both SEM and TEM micrographs. The size of the porous particles is observed to be within the range of 30−60 nm from SEM which might be due to the presence of agglomerated particles. The TEM micrographs (Figure 2c,f) have confirmed that the synthesized nanomilled n-HAp has plate-like structures and the porous size of the n-HAp powder particles is within the range of 10−30 nm which also complies with the results from the XRD. In addition to that, it is observed that CA-n-HAp is more porous compared to PP-n-HAp.

3.1.3. Surface Analysis of n-HAp Powder. The XPS spectra obtained from survey scan of the n-HAp powder from CA and PP scales are shown in Figure 3a,b, respectively. In addition to Ca, P, and O, small peaks related to C (1s), which are also called "adventitious carbon" were found in both the samples with 11 and 19% in CA-n-HAp and PP-n-HAp, respectively.[40] Small impurity of Na with 0.6% was found in CA-n-HAp which might be due to the contamination of sample during the process. The surface Ca/P atomic ratios associated with O(1s) were analyzed. The oxygen intensity of CA-n-HAp (Figure 3a) is observed to be higher than that of PP-n-HAp (Figure 3b) which might favor the cell adhesion. The Ca/P ratio of CA-n-HAp powder was found to be 1.17, whereas the PP-n-HAp powder has a C/P ratio of 1.37. Generally, the stoichiometric apatite $[Ca_{10}(PO_4)_6(OH)_2]$ has a Ca/P ratio of 1.67.[10] The Ca/P ratio of the synthesized n-HAp powders suggest that the n-HAp obtained is calcium deficient. However, the structural deficiency of the n-HAp powder does not influence the crystalline formulation as shown in XRD spectra (Figure 1). It is to be noted that the level of deficiency plays an important role in the catalysis reaction involving alcohols. The rate of catalytic reaction increases with the increase in calcium deficiency of n-HAp and is highly suitable for biomedical applications.[41]

3.2. Characterization of PCL Fibers. *3.2.1. Morphology of Fibers.* The characterization of synthesized n-HAp powder has met the desired requirements to be infused as filler into the polymer matrix. The synthesized n-HAp powder was reinforced into the PCL solution with 1, 3, and 5 wt % to obtain fibrous nonwoven mats. The SEM micrographs of thus obtained forcespun nonwoven mats are shown in Figure 4. Randomly oriented three-dimensional mesh of homogeneous fibers was observed for all the fiber samples. The diameter of the fibers obtained at 6000 rpm was evaluated using Gaussian distribution for which the frequency of the estimated distribution of fibers is shown in the inset of the micrographs, and the results are tabulated in Table 1. Figure 4a represents neat PCL fiber, Figure 4b−d shows the PCL fibers with CA-n-Hap, and Figure 4e−g represents fibers with PP-n-HAp. The diameters of the fibers were small and lie between 300 and 600 nm compared to the fibers that were obtained with only one solvent (chloroform) which were around 1.5−4 μm.[35] This might be due to the usage of two solvents which have different evaporation rates. As the filler content increases, the diameter of the fibers also increases. The fibers with PP-n-HAp have shown a relatively small diameter compared to fibers with CA-n-HAp for 1 and 3 wt %. Furthermore, due to the increase in the agglomerations with filler content, the fibers became nonuniform, showing thick and thin fibers, as shown in Figure 4d,g. Although the fiber diameter was less, beads were observed along with the fibers. The solidification time between the ejection of polymer solution from the spinneret and the deposition of the solution on to the collector influences the beading of the fibers.[34]

Table 1. Mean Fiber Diameter of the Forcespun PCL Fibers for Various Rotational Speeds

HAp wt %	PCL-CA-n-HAp mean diameter (μm)	PCL-PP-n-HAp mean diameter (μm)
PCL neat (0 wt %)	0.342 ± 0.014	0.342 ± 0.014
1 wt %	0.385 ± 0.008	0.377 ± 0.012
3 wt %	0.445 ± 0.015	0.426 ± 0.006
5 wt %	0.547 ± 0.009	0.577 ± 0.024

3.2.2. Raman Analysis of Fibers. The band position assignment of the fibers infused with n-HAp was analyzed using Raman spectroscopy for CA and PP and is shown in Figure 5 along with the n-HAp powder and neat PCL. The neat PCL fibers exhibit several narrow peaks pertaining to 913.8 and 955 cm^{-1}(C−COO stretch), 1034−1105 cm^{-1} (C−C stretch), 1287−1340 cm^{-1} (CH_2 twist), 1412−1438 cm^{-1} (CH_2 bend), and 1721 cm^{-1}(C═O stretch).[42,43] The characteristic peaks for n-HAp were observed at around 430, 580, and 960 cm^{-1} for both CA and PP n-HAp as shown in Figure 5a,b and the ν_1 phosphate PO_4^{3-}dominates the n-HAp spectrum.[44,45] The n-HAp bands in PCL-n-HAp fibers were dominated by PCL peaks as anticipated. The P−O vibrational (430 cm^{-1}) and deformation (580 cm^{-1}) did not exhibit any noticeable influence on PCL-n-HAp fibers. However, a slight rise in the intensity of the peaks at 958−960 cm^{-1} was observed for PCL-n-HAp fibers. Especially, the rise in the intensity is evident for 5 wt % PCL-n-HAp fibers for both CA and PP samples and thus confirms the presence of n-HAp powder in the polymer matrix. This is also complemented by the presence of peaks due to ν_3 PO_4^{3-} (P−O asymmetric valence) at 1032 and 1044 cm^{-1} for CA and PP, respectively. Figure 5a exhibits the peaks with increased intensity corresponding to 1095 cm^{-1} of CA-n-HAp which suggests that CA-n-HAp favors A-type substitution of carbonate (ν_1 CO_3^{2-}) ion.[44] Meanwhile, PP-n-HAp has shown the Raman peak in the region of 1075, which suggests the ν_1 CO_3^{2-} B-type substitution. Furthermore, significant increase in the intensity of the peaks corresponding to the carbonate ion band was observed. The amide III and C−H bending bands of n-HAp resulted in the distinct peaks related to C−H bending of PCL-n-HAp fibers which are remarkably evident. Thus, the Raman analysis has confirmed the presence of conformational isomerism and some possible intercessions of n-HAp in PCL-n-HAp fibers.

3.2.3. Thermal Analysis of PCL-n-HAp Fibers. The thermal stability, properties, and behavior of the PCL-n-HAp fibers were analyzed from the TGA and DSC characteristic curves. The initial decomposition temperature, final decomposition temperature, major degradation temperature, weight change during to the major degradation, and residue left at 450 and 700 °C are evaluated and are summarized in Table 2. Figure 6 shows TGA curves with a single-step degradation process that lies between 368 and 418 °C for all the fiber samples with major degradation temperature around 395 °C. Figure 6a,b shows the characteristic weight loss curves and derivative

https://doi.org/10.1021/acsomega.1c05593
ACS Omega 2022, 7, 8323−8335

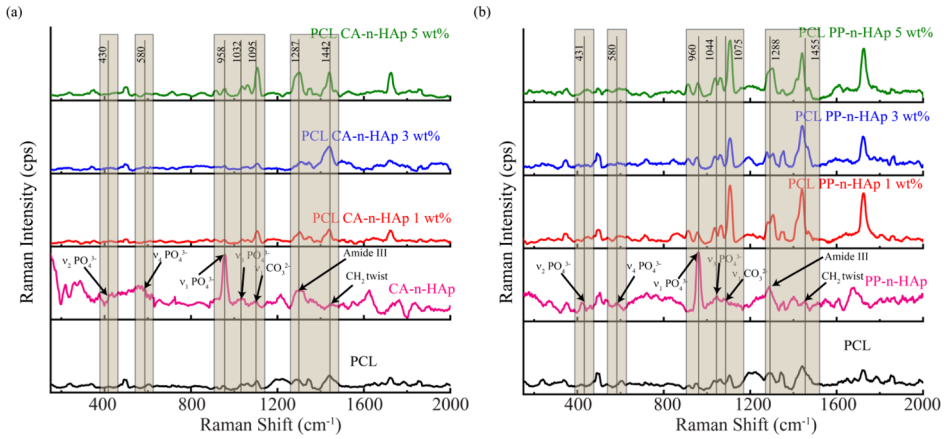

Figure 5. Raman spectra of PCL-n-HAp fibers with 1, 3, and 5 wt % for (a) CA-n-HAp and (b) PP-n-HAp. The numerical data of the peaks presented correspond to the n-HAp spectrum of CA and PP.

Table 2. Summary of the Data from TGA

PCL-n-HAp wt %	initial decomposition temperature (°C)	final decomposition temperature (°C)	major degradation temperature (°C)	weight change for major degradation (%)	residue left at 450 °C (%)	residue left at 700 °C (%)
neat (0 wt %)	370.31	413.56	395.49	98.94	2.23	0.07
CA-n-HAp 1 wt %	372.13	417.38	397.93	98.86	2.21	0.89
CA-n-HAp 3 wt %	371.7	415.75	395.92	97.61	3.40	1.8
CA-n-HAp 5 wt %	370.97	414.91	395.3	95.73	5.8	3.7
PP-n-HAp 1 wt %	372.7	417.46	397.72	98.92	1.69	0.58
PP-n-HAp 3 wt %	368.69	414.88	395.11	97.38	3.77	2.26
PP-n-HAp 5 wt %	368.37	414.6	395.05	96.3	5.15	3.33

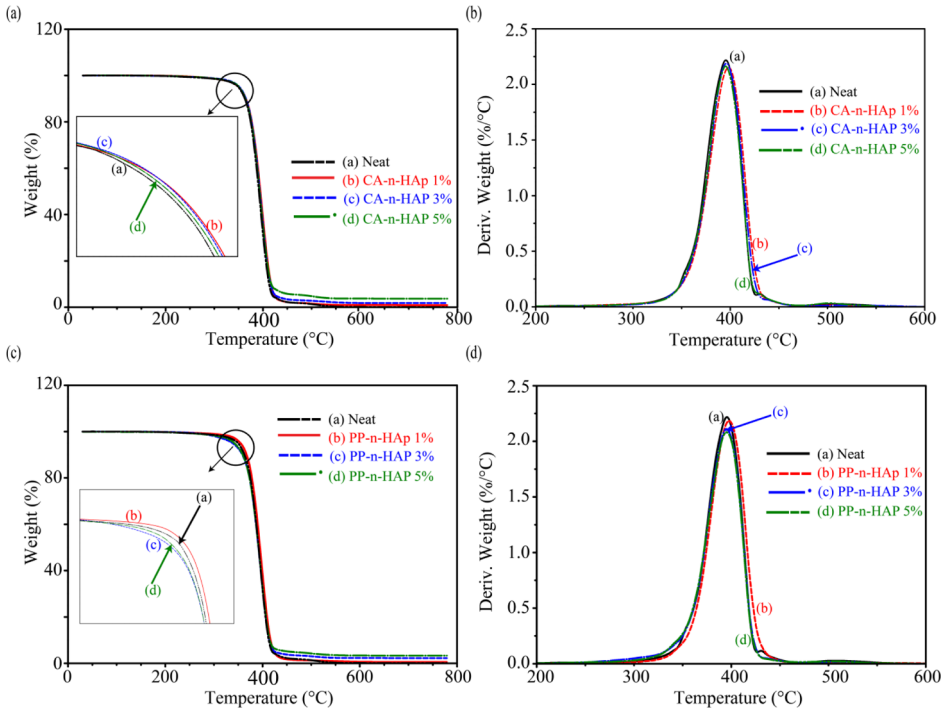

Figure 6. TGA of PCL fibers with CA-n-HAp and PP-n-HAp showing (a,c) weight change, and (b,d) derivative weight change, respectively.

weight loss curves for CA-n-HAp infused fibers and Figure 6c,d represents PP-n-Hap-infused fibers, respectively. Nominal weight loss of around 5% was observed in the initial stages, that is, from 30 to 350 °C for all samples of CA-n-HAp and 1

https://doi.org/10.1021/acsomega.1c05593
ACS Omega 2022, 7, 8323−8335

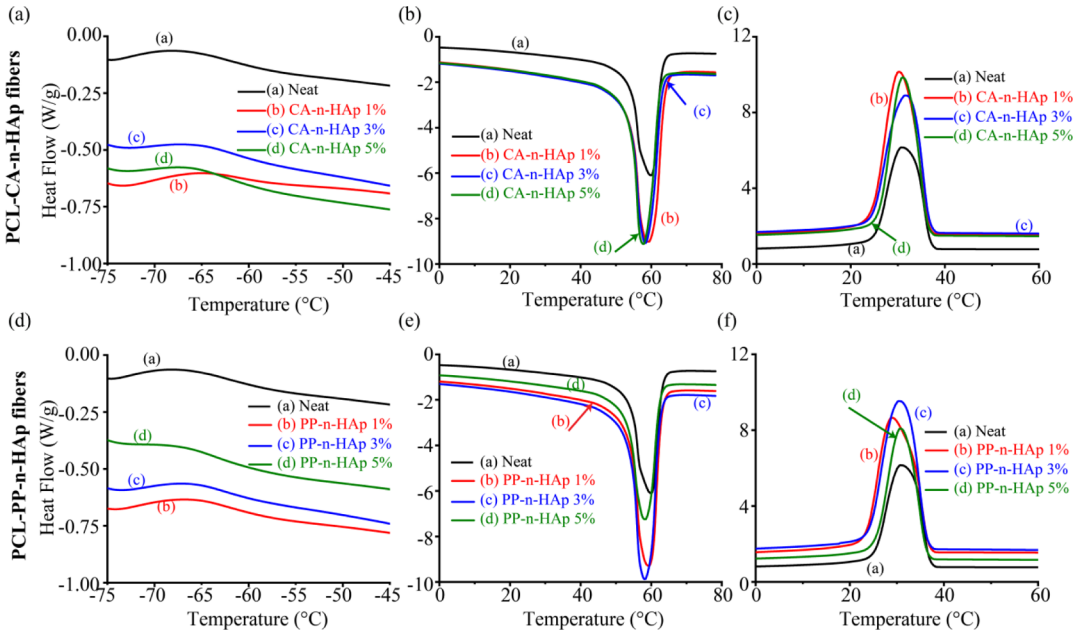

Figure 7. DSC thermographs showing (a,d) glass transition temperature, (b,e) melting endotherms, and (c,f) crystallization temperatures for PCL fibers with CA-n-HAp and PP-n-HAp, respectively.

Table 3. DSC Analysis for the PCL Fibers Obtained at Various Rotational Speeds

			second heating		cooling		
PCL-n-HAp wt %	glass transition temperature T_g (°C)	first heating T_m (°C)	T_m (°C)	ΔH_m (J/g)	T_c (°C)	ΔH_c (J/g)	% crystallinity (χc)
neat (0 wt %)	−62.4	60.48	59.25	58.22	30.57	58.79	0.41
CA-n-HAp 1 wt %	−61.3	61.23	59.24	59.34	30.62	58.73	0.44
CA-n-HAp 3 wt %	−61.9	60.83	58.35	61.81	31.66	62.41	0.43
CA-n-HAp 5 wt %	−62	60.94	57.8	59.81	31.07	59.46	0.25
PP-n-HAp 1 wt %	−61.9	59.91	59.32	60.54	28.92	61.12	0.42
PP-n-HAp 3 wt %	−62.3	59.81	58.15	58.85	30.48	58.42	0.31
PP-n-HAp 5 wt %	−63.6	60.12	58.24	55	30.78	55.32	0.23

wt % PP-n-HAp which corresponds to the loss of moisture except for PP-n-HAp which showed a weight loss of around 7% for both 3 and 5 wt % of filler content. It can be presumed that PP-n-HAp has relatively high moisture absorbance capacity compared to CA-n-HAp and the hydrophobic nature of PCL can be compensated with reinforcement of PP-n-HAp.[46] The initial decomposition temperature has increased from 370° of neat fibers to around 373° of 1 wt % CA-n-HAp and PP-n-HAp. The major degradation temperature also has shown considerable increase from 395° of neat fibers to around 398° of 1 wt % CA-n-HAp and PP-n-HAp (Figure 6b,d), suggesting that infusing a low amount of filler delays the decomposition and thus enhances the thermal stability of the composite. With the further increase in the filler content, the major degradation temperature reduces and is more or less equal to that of major degradation temperature of neat fibers as shown for the curves (c) and (d) in Figure 6b,d. Although no significant change is observed for major degradation temperatures for other filler concentrations compared to neat fibers, the weight change during the major degradation has decreased with the increase in the filler percentages of both CA-n-HAp and PP-n-Hap, suggesting the reduced loss of the organic content. This also complies with the results that are observed for the residue left at 450 °C which shows that 5 wt % has a higher amount of residue of around 3.7% for CA-n-HAp and 3.3% for PP-n-HAp. Finally, the residue left at 700 °C was observed which showed a similar trend to that of residue left at 450 °C. Overall, the results confirm the presence of n-HAp in the polymer matrix and also suggest that infusing the n-HAp into PCL will enhance the thermal stability of the PCL while also improving its moisture adsorbance capacity which favors the cell attachment and infiltration.[16] Furthermore, the degradation temperatures suggest that PCL-n-HAp scaffolds can be fabricated conveniently without any material losses.[47]

Furthermore, to understand the thermal behavior of PCL-n-HAp fibers, DSC analysis was performed and the thermographs are shown in Figure 7. The glass transition (T_g), crystallization (T_c), and enthalpy of crystallization (ΔH_c) were evaluated from the first heating curve, whereas the melting (T_m) and enthalpy of fusion (ΔH_m) were evaluated from the second heating cycle of the DSC endotherms and are tabulated in Table 3. The glass transition temperature has increased for all the fiber samples compared to neat PCL except for 5 wt % of PP-n-HAp. The increase in the T_g with the infusion of n-HAp powder suggests that the large specific surface area of the filler particles have successfully restricted the mobility of polymer chains, thus increasing the resistance.[35] However, for the 5 wt % PP-n-HAp sample might have highly agglomerated particles as observed from the mean diameter of the fibers from SEM, might have decreased T_g. Although there is a minute increment for CA-n-HAp samples in the melting point from the first heating curve as shown in Table 3, there is no

https://doi.org/10.1021/acsomega.1c05593
ACS Omega 2022, 7, 8323−8335

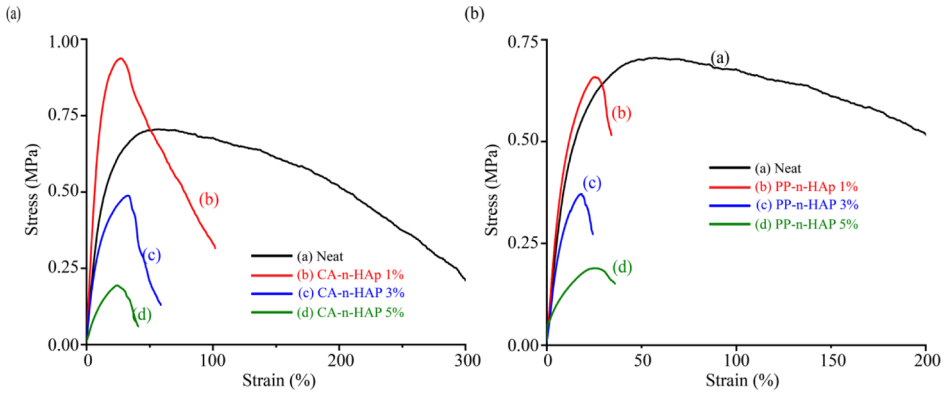

Figure 8. Averaged stress−strain curves of PCL microfiber mats obtained for (a) CA-n-HAp and (b) PP-n-HAp.

significant shift in the melting point temperatures of both first and second heating curve and also in the crystallization temperatures. The melting points from the second heating curve lie in the range of 58−59 °C, whereas the crystallization temperatures range from 29 to 32 °C. However, all the CA-n-HAp samples have shown high crystallization temperatures compared to that of neat PCL sample surmising that the CA-n-HAp can act as nucleating agent increasing the crystallization rate and ability of the PCL.[48,49] This is also confirmed by the crystallinity of the samples. The crystallinity was calculated from the following equation

$$\chi_c = \frac{\Delta H_m - \Delta H_c}{\Delta H_f}$$

where χ_c is the crystallinity and ΔH_f is the enthalpy of fusion of 100% crystalline sample (139.5 J/g for PCL). The crystallinity of the fibers has shown increment for 1 and 3 wt % of CA-n-HAp and 1 wt % of PP-n-HAp. The observed results are in agreement with the TGA results following major degradation temperature. However, as the filler content increases, the crystallinity decreases. The formation of hydrogen bonds between the PCL and n-HAp which might have resulted in restricted mobility of the polymer chain might have reduced the crystallinity.[46,50]

3.3. Tensile Test Analysis. The typical stress−strain curves for the forcespun PCL fibers infused with CA and PP n-HAp and obtained at 6000 rpm are shown in Figure 8. Six samples were tested for each case and the average of the consistent four samples was considered for each sample. The tensile properties of the forcespun PCL fiber mats are tabulated in Table 4. The Young's modulus of the neat PCL fibers was found to be 4.63 MPa and thus agrees with the results that were reported in the literature for electrospun fiber mats which lie within 3.5 and 6 MPa.[51−53] The results obtained are in agreement with the finding that the mechanical performance of PCL fibers can be improved with the blending of composites at low filler loadings.[54] The PCL fibers with 1 wt % of n-HAp from CA and PP scales have shown a significant increase in the Young's modulus as well as the tensile strength. The optimal Young's modulus was found to be 8.21 MPa for 1 wt % of CA-n-HAp, which is approximately the same as the results obtained by Heo et al. for PCL-n-HAp scaffolds and is almost twice that of the neat PCL fibers.[22] The tensile strength also increased with the reinforcement of n-HAp in PCL.[55,56] The enhanced tensile properties of the fibers might be due to the formation of temporary intermolecular bonds during the tensile loading, promoting the alignment and orientation of

Table 4. Summary of the Tensile Test Analysis for Forcespun PCL Fibers at Various Rotational Speeds

CL-n-HAp wt %	Young's Modulus (MPa)	tensile Strength (MPa)	strain at *F*max(%)
neat (0 wt %)	4.63 ± 0.38	0.72 ± 0.02	57.93 ± 11.64
CA-n-HAp 1 wt %	8.21 ± 0.50	0.95 ± 0.04	27.89 ± 3.20
CA-n-HAp 3 wt %	3.45 ± 0.24	0.49 ± 0.05	35.41 ± 3.77
CA-n-HAp 5 wt %	1.28 ± 0.11	0.21 ± 0.03	28.78 ± 4.26
PP-n-HAp 1 wt %	5.37 ± 1.60	0.68 ± 0.19	27.44 ± 3.61
PP-n-HAp 3 wt %	3.62 ± 1.00	0.39 ± 0.06	21.32 ± 3.84
PP-n-HAp 5 wt %	1.46 ± 0.58	0.21 ± 0.02	28.40 ± 6.30

nanoparticles within the polymer chains, thus increasing the strength of the fibers.[57] This is also evident from the increase in glass transition temperature and the crystallinity of the fibers, as shown in Table 3. However, the elongation (strain) at maximum force has decreased for PCL-n-HAP fibers compared to that of the neat fibers. This is anticipated as the HAp being ceramic is hard and brittle and thus increases the brittleness of the fibers.

Although the crystallinity is high for 3 wt % of CA-n-HAp compared to the neat fibers, the tensile properties decreased for 3 wt % (Figure 8a). Furthermore, it is also observed that, the tensile properties of the PCL-n-HAp fibers were inferior to the properties of the PCL-n-HAp fibers with single solvent (chloroform) which were reported in Kodali et al.[35] This suggests that high porosity might be induced within the fibrous membranes due to the distinct evaporation rates of chloroform and THF, which resulted in the decrement of the Young's modulus and tensile strength. Furthermore, with the increase in the filler content, the surface roughness of the fibers increased with the induced porosity which is evident from Figure 4d,g. The high filler contents also might have contributed to the inhomogeneous dispersion of filler which resulted in the nonuniform structure of the fibers resulting in beads. These beaded structures also might have contributed to the deterioration of mechanical properties. Owing to the particle agglomerations at higher filler loadings of n-HAp, the crystallinity of the fibers has decreased due to the impeded mobility of n-HAp particles.[58] Thus, the energy dissipation ability of the n-HAp particles decreases with increased concentration at the PCL-n-HAp interface and thus might

https://doi.org/10.1021/acsomega.1c05593
ACS Omega 2022, 7, 8323−8335

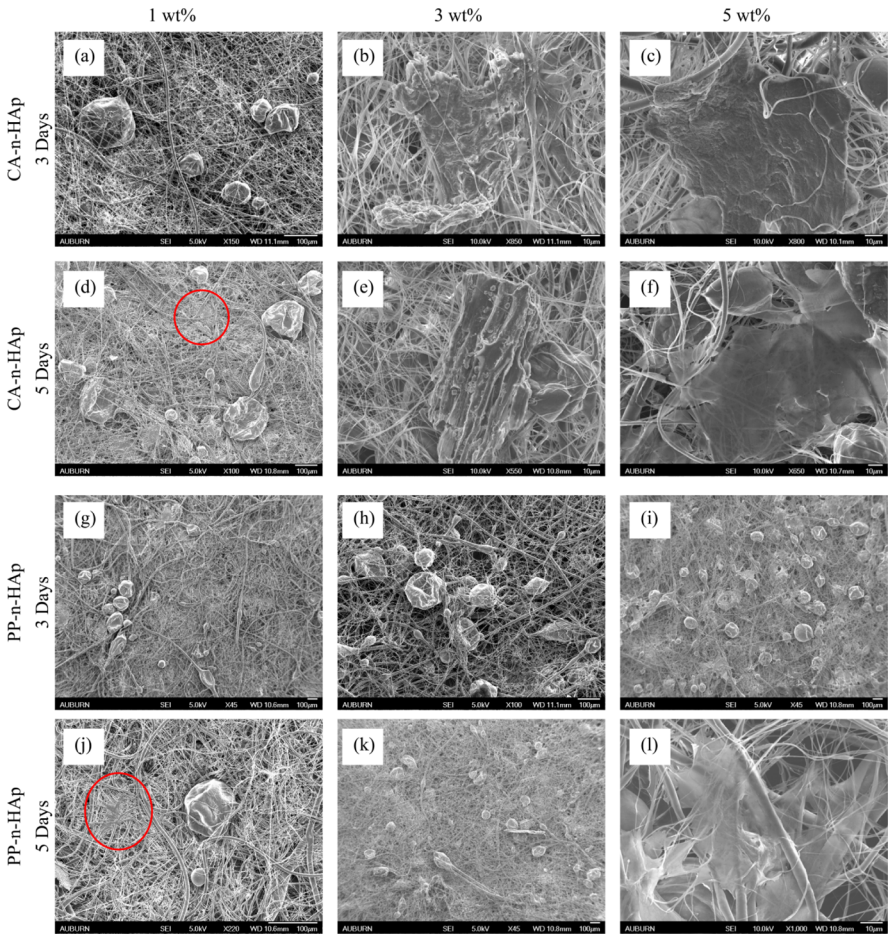

Figure 9. SEM micrographs of cell adhesion on PCL-n-HAp scaffolds for CA-n-HAp 3 days (a) 1, (b) 3, and (c) 5 wt %; CA-n-HAp 5 days (d) 1, (e) 3, and (f) 5 wt %; PP-n-HAp 3 days (g) 1, (h) 3, and (i) 5 wt %; and PP-n-HAp 5 days (j) 1, (k) 3, and (l) 5 wt %.

have resulted in the downtrend of mechanical properties.[57,59,60]

3.4. Cell Proliferation Analysis. To evaluate the potential of developed fibrous scaffolds for bone and dental regeneration applications, the cell adhesion on the seeded scaffolds was analyzed by SEM for 3 and 5 days. Figure 9 shows the SEM micrographs of the seeded scaffolds that were immersed in culture media for 3 and 5 days for CA-n-HAp and PP-n-HAp. The neat fibrous scaffolds did not exhibit any cell growth and hence were not discussed in this section. The smooth surface of the scaffolds before seeding the cells began to become coarse after seeding with the cells with subsequent growing of the cells and masking the micro pores. After 3 days, a thin layer of cells can be seen on every scaffold surface as shown in Figure 9 and has shown agglomeration on day 5. The PCL scaffolds infused with 1 wt % CA and PP n-HAp have shown imperceptible growth from 3 to 5 days [figures (a), (d), (g), and (j)]. However, it can be observed that the cells are attached which suggests that even the low filler loading of n-HAp favors the cell growth. As the filler loading increased to 3 wt %, cell growth is noticeably visible from 3 to 5 days for both CA and PP n-HAp [figures (b), (e), (h), and (k)]. The scaffolds with 5 wt % n-HAp have shown incredible cell growth from 3 to 5 days [figures (c), (f), (i), and (l)] where the scaffolds were covered by layer of cells. From the cell adhesion and proliferation studies it is evident that both scaffolds with 3 and 5 wt % n-HAp for CA and PP are suitable for cell adhesion and spreading. The seeded cells exhibited formidable adhesion with filopodia attachment on scaffold surface from day 3 in both types. The influence of n-HAp is evident as the scaffolds with the increase in the percentage of n-HAp (3 and 5 wt % HAp) showed an outstanding growth of cells from day 3 of the study. The temporal changes observed are attachment of cells to the surface and colonization of cells on the surface and into the pores of the scaffold. The cells exhibited excellent attachment for 5 wt % scaffolds from day 3 and had full compatibility with the scaffolds. The cell growth was not completely uniform which might be due to the differences in the surface morphology of scaffold and seeding density of the cells. These hFOB cells show similar growth pattern when studied on 3D-printed scaffolds.[61] The FESEM images suggest that these scaffolds can serve as a domain where osteoblasts can grow, attach, and proliferate. When biomaterials are modified into biocompatible Hap, they acquire better biological properties due to the presence of cations such as Mg^{2+}, Zn^{2+}, Al^{3+}, K^{+}, and Na^{+} along with anions such as Cl^{-} and F^{-}. These cations and anions in combination are reported to aid in rapid bone regeneration. To further understand the behavior of these scaffolds in human body, they must be studied by incubating for longer time periods which is considered for future study. However, it is to be noted that although increasing the n-HAp filler loading improves the bioactive performance of the scaffolds, it also compromises the mechanical properties of the scaffolds due to agglomeration, as shown in Table 4. However, if the mechanical properties are adequate enough and are similar to the host and the bioactive

https://doi.org/10.1021/acsomega.1c05593
ACS Omega 2022, 7, 8323−8335

performance is of main concern, high amounts of filler loadings are suggested based on the results.[30]

4. CONCLUSIONS

The n-HAp powders synthesized from CA and PP fish scales were characterized using XRD, SEM, TEM, and XPS. The XRD results conform the standard n-HAp and also suggest the crystallite size in the nano range. The SEM and TEM results further comprehend that the size of the synthesized n-HAp powder is in the nano range and show that the synthesized particles are irregular and are porous in nature. The forcespinning technique that utilizes centrifugal forces was exercised to successfully develop PCL-n-HAp fibrous scaffolds. The influence of the n-HAp from CA and PP scales with various filler loadings on PCL-n-HAp scaffolds was thoroughly investigated using thermal, mechanical, and biological studies. Although the diameter of the fibers increased with the increase in the n-HAp content, the size of the fibers lies within the nano range. The fibers obtained were nonuniform and porous and have beads which might be due to the usage of two solvents chloroform and THF which has two different evaporation rates. The Raman analysis confirmed the presence of n-HAp in the developed fibers and also suggested some possible interferences of n-HAp in the polymer matrix. The onset and major degradation temperatures have noticeable increment for 1 wt % of CA-n-HAp and PP-n-HAp. The residue left has increased with the increase in the filler content. The glass transition and crystallinity increases for 1 wt % of CA-n-HAp and PP-n-HAp and further decreases for 3 and 5 wt %. The tensile tests also follow a similar trend which complies with the crystallinity of the fibers. However, the thermal and mechanical properties observed would be sufficient and favorable for biomedical applications. The cell studies have shown outstanding cell growth and adhesion for 5 wt % of CA-n-HAp and PP-n-HAp. Detailed investigation of the intensity of cell growth and the differences due to CA and PP n-HAp is intended for future study. Overall, the study suggests that the fish scale-based n-HAp when infused with PCL can serve as a potential material for biomedical applications that is suitable for wound healing and tissue engineering.

AUTHOR INFORMATION

Corresponding Author

Vijaya K. Rangari − *Department of Materials Science Engineering, Tuskegee University, Tuskegee, Alabama 36088, United States;* orcid.org/0000-0002-3962-1686; Email: vrangari@tuskegee.edu

Authors

Deepa Kodali − *Department of Materials Science Engineering, Tuskegee University, Tuskegee, Alabama 36088, United States*

Vincent Hembrick-Holloman − *Department of Materials Science Engineering, Tuskegee University, Tuskegee, Alabama 36088, United States*

Dilip Reddy Gunturu − *College of Veterinary Medicine Nursing and Allied Health, Pathobiology, Tuskegee University, Tuskegee, Alabama 36088, United States*

Temesgen Samuel − *College of Veterinary Medicine Nursing and Allied Health, Pathobiology, Tuskegee University, Tuskegee, Alabama 36088, United States*

Shaik Jeelani − *Department of Materials Science Engineering, Tuskegee University, Tuskegee, Alabama 36088, United States*

Complete contact information is available at: https://pubs.acs.org/10.1021/acsomega.1c05593

Notes

The authors declare no competing financial interest.

ACKNOWLEDGMENTS

The authors acknowledge financial support from NSF-CREST #1735971, NSF-EPSCoR # 1655280, NSF-RISE # 1459007, NSF-MRI, #1531934, and grant #G12MD007585. The authors also acknowledge Dr. Paul Baker from University of Alabama in Birmingham for his support in XPS studies.

REFERENCES

(1) Coppola, D.; Lauritano, C.; Palma Esposito, F.; Riccio, G.; Rizzo, C.; de Pascale, D. Fish Waste: From Problem to Valuable Resource. *Mar. Drugs* **2021**, *19*, 116−39.

(2) United Nations. *Special Edition*; Progress towards the Sustainable Development Goals, 2019.

(3) FAO. *The State of World Fisheries and Aquaculture 2020*; FAO, 2020.

(4) Mondal, S.; Hoang, G.; Manivasagan, P.; Moorthy, M. S.; Kim, H. H.; Vy Phan, T. T.; Oh, J. Comparative Characterization of Biogenic and Chemical Synthesized Hydroxyapatite Biomaterials for Potential Biomedical Application. *Mater. Chem. Phys.* **2019**, *228*, 344−356.

(5) Wangkheirakpam, M. R.; Mahanand, S. S.; Majumdar, R. K.; Sharma, S.; Netam, S. Fish Waste Utilization with Reference to Fish Protein Hydrolysate-A Review Food Processing View Project Fish Protein Hydrolysate of *Wallago Attu* View Project. *Fish. Technol.* **2019**, *56*, 169−178.

(6) Liu, W.-K.; Liaw, B.-S.; Chang, H.-K.; Wang, Y.-F.; Chen, P.-Y. From Waste to Health: Synthesis of Hydroxyapatite Scaffolds From Fish Scales for Lead Ion Removal. *J. Occup. Med.* **2017**, *69*, 713−718.

(7) Athinarayanan, J.; Periasamy, V. S.; Alshatwi, A. A. Simultaneous Fabrication of Carbon Nanodots and Hydroxyapatite Nanoparticles from Fish Scale for Biomedical Applications. *Mater. Sci. Eng. C* **2020**, *117*, 111313.

(8) Paul, S.; Pal, A.; Choudhury, A. R.; Bodhak, S.; Balla, V. K.; Sinha, A.; Das, M. Effect of Trace Elements on the Sintering Effect of Fish Scale Derived Hydroxyapatite and Its Bioactivity. *Ceram. Int.* **2017**, *43*, 15678−15684.

(9) Wu, C.-S.; Wu, D.-Y.; Wang, S.-S. Biodegradable Composite Nanofiber Containing Fish-Scale Extracts. *ACS Appl. Bio Mater.* **2021**, *4*, 462−469.

(10) Agbeboh, N. I.; Oladele, I. O.; Daramola, O. O.; Adediran, A. A.; Olasukanmi, O. O.; Tanimola, M. O. Environmentally Sustainable Processes for the Synthesis of Hydroxyapatite. *Heliyon* **2020**, *6*, No. e03765.

(11) Sathiskumar, S.; Vanaraj, S.; Sabarinathan, D.; Bharath, S.; Sivarasan, G.; Arulmani, S.; Preethi, K.; Ponnusamy, V. K. Green synthesis of biocompatible nanostructured hydroxyapatite from Cirrhinus mrigala fish scale—A biowaste to biomaterial. *Ceram. Int.* **2019**, *45*, 7804−7810.

(12) Mohd Pu'ad, N. A. S.; Abdul Haq, R. H.; Mohd Noh, H.; Abdullah, H. Z.; Idris, M. I.; Lee, T. C. Nano-Size Hydroxyapatite Extracted from Tilapia Scale Using Alkaline Heat Treatment Method. *Mater. Today: Proc.* **2020**, *29*, 218−222.

(13) Mondal, S.; Pal, U. 3D Hydroxyapatite Scaffold for Bone Regeneration and Local Drug Delivery Applications. *J. Drug Deliv. Sci. Technol.* **2019**, *53*, 101131.

(14) Surya, P.; Nithin, A.; Sundaramanickam, A.; Sathish, M. Synthesis and Characterization of Nano-Hydroxyapatite from

https://doi.org/10.1021/acsomega.1c05593
ACS Omega 2022, 7, 8323−8335

Sardinella Longiceps Fish Bone and Its Effects on Human Osteoblast Bone Cells. *J. Mech. Behav. Biomed. Mater.* **2021**, *119*, 104501.
(15) Hasan, M. R.; Mohd Yasin, S. N.; Mohd Yasin, N. S.; Mohd Ghazali, M. S.; Mohtar, N. F. Proximate and Morphological Characteristics of Nano Hydroxyapatite (Nano Hap) Extracted From Fish Bone. *J. Sustainability Sci. Manage.* **2020**, *15*, 9−21.
(16) Chocholata, P.; Kulda, V.; Babuska, V. Fabrication of Scaffolds for Bone-Tissue Regeneration. *Mater.*. **2019**, *12* (). DOI: 10.3390/ma12040568.
(17) Deb, P.; Deoghare, A. B.; Barua, E. Poly Ethylene Glycol/Fish Scale-Derived Hydroxyapatite Composite Porous Scaffold for Bone Tissue Engineering. *IOP Conf. Ser. Mater. Sci. Eng.* **2018**, *377* (). DOI: 10.1088/1757-899X/377/1/012009.
(18) Deb, P.; Barua, E.; Deoghare, A. B.; Lala, S.; Das, D. Development of Bone Scaffold Using Puntius Conchonius Fish Scale Derived Hydroxyapatite: Physico-Mechanical and Bioactivity Evaluations. *Ceram. Int.* **2019**, *45*, 10004−10012.
(19) Wijedasa, N. P.; Broas, S. M.; Daso, R. E.; Banerjee, I. A. Varying Fish Scale Derived Hydroxyapatite Bound Hybrid Peptide Nanofiber Scaffolds for Potential Applications in Periodontal Tissue Regeneration. *Mater. Sci. Eng. C* **2020**, *109*, 110540.
(20) Jin, S.; Sun, F.; Zou, Q.; Huang, J.; Zuo, Y.; Li, Y.; Wang, S.; Cheng, L.; Man, Y.; Yang, F.; Li, J. Fish Collagen and Hydroxyapatite Reinforced Poly(lactide-co-glycolide) Fibrous Membrane for Guided Bone Regeneration. *Biomacromolecules* **2019**, *20*, 2058−2067.
(21) Li, L.; Zuo, Y.; Zou, Q.; Yang, B.; Lin, L.; Li, J.; Li, Y. Hierarchical Structure and Mechanical Improvement of an N-HA/GCO-PU Composite Scaffold for Bone Regeneration. *ACS Appl. Mater. Interfaces* **2015**, *7*, 22618−22629.
(22) Heo, S. Y.; Ko, S. C.; Oh, G. W.; Kim, N.; Choi, I. W.; Park, W. S.; Jung, W. K. Fabrication and characterization of the 3D-printed polycaprolactone/fish bone extract scaffolds for bone tissue regeneration. *J. Biomed. Mater. Res., Part B* **2019**, *107*, 1937−1944.
(23) Pon-On, W.; Suntornsaratoon, P.; Charoenphandhu, N.; Thongbunchoo, J.; Krishnamra, N.; Tang, I. M. Synthesis and Investigations of Mineral Ions-Loaded Apatite from Fish Scale and PLA/Chitosan Composite for Bone Scaffolds. *Mater. Lett.* **2018**, *221*, 143−146.
(24) Vandana, B.; Syamala, P.; Venugopal, D. S.; Sk, S. R. K. I.; Venkateswarlu, B.; Jagannatham, M.; Kolenčík, M.; Ramakanth, I.; Dumpala, R.; Sunil, B. R. Magnesium/Fish Bone Derived Hydroxyapatite Composites by Friction Stir Processing: Studies on Mechanical Behaviour and Corrosion Resistance. *Bull. Mater. Sci.* **2019**, *42*, 122.
(25) Sivasankaran, P. N.; Ward, T. A. Spatial Network Analysis to Construct Simplified Wing Structural Models for Biomimetic Micro Air Vehicles. *Aerosp. Sci. Technol.* **2016**, *49*, 259−268.
(26) Nikolova, M. P.; Chavali, M. S. Recent Advances in Biomaterials for 3D Scaffolds: A Review. *Bioact. Mater.* **2019**, *4*, 271−292.
(27) Malysheva, K.; Kwaśniak, K.; Gnilitskyi, I.; Barylyak, A.; Zinchenko, V.; Fahmi, A.; Korchynskyi, O.; Bobitski, Y. Functionalization of Polycaprolactone Electrospun Osteoplastic Scaffolds with Fluorapatite and Hydroxyapatite Nanoparticles: Biocompatibility Comparison of Human versus Mouse Mesenchymal Stem Cells. *Mater.*. **2021**, *14* (). DOI: 10.3390/ma14061333.
(28) Asghari, F.; Samiei, M.; Adibkia, K.; Akbarzadeh, A.; Davaran, S. Biodegradable and Biocompatible Polymers for Tissue Engineering Application: A Review. *Artif. Cells, Nanomed., Biotechnol.* **2017**, *45*, 185−192.
(29) del Ángel-Sánchez, K.; Ulloa-Castillo, N. A.; Segura-Cárdenas, E.; Martinez-Romero, O.; Elías-Zuñiga, A. Design, fabrication, and characterization of polycaprolactone (PCL)-TiO2-collagenase nanofiber mesh scaffolds by Forcespinning. *MRS Commun.* **2019**, *9*, 390−397.
(30) Hajiali, F.; Tajbakhsh, S.; Shojaei, A. Fabrication and Properties of Polycaprolactone Composites Containing Calcium Phosphate-Based Ceramics and Bioactive Glasses in Bone Tissue Engineering: A Review. *Polym. Rev.* **2018**, *58*, 164−207.
(31) Padilla-Gainza, V.; Morales, G.; Rodríguez-Tobías, H.; Lozano, K. Forcespinning technique for the production of poly(d , l -lactic acid) submicrometer fibers: Process-morphology-properties relationship. *J. Appl. Polym. Sci.* **2019**, *136*, 47643.
(32) McEachin, Z.; Lozano, K. Production and Characterization of Polycaprolactone Nanofibers via Forcespinning Technology. *J. Appl. Polym. Sci.* **2012**, *126*, 473−479.
(33) Sarkar, K.; Gomez, C.; Zambrano, S.; Ramirez, M.; De Hoyos, E.; Vasquez, H.; Lozano, K. Electrospinning to Forcespinning. *Mater. Today* **2010**, *13*, 12−14.
(34) Kodali, D.; Syed, F.; Jeelani, S.; Rangari, V. K. Fabrication and Characterization of Forcespun Polycaprolactone Microfiber Scaffolds. *Mater. Res. Express* **2020**, *7* (). DOI: 10.1088/2053-1591/abcac1.
(35) Kodali, D.; Hembrick-Holloman, V.; Jeelani, S.; Rangari, V. K. Thermomechanical properties of forcespun polycaprolactone fibers infused with fish scale-based hydroxyapatite. In *Plant and Animal Based Composites*; Kumar, K., Davim, J. P., Eds.; De Gruyter: Berlin, Boston, 2021; pp 127−148.
(36) ElectrospinTech. Tensile testing of electrospun nanofiber membrane, http://electrospintech.com/SOP-ES2002.html#.XiJRKf5KiUl (accessed 03 July 2013).
(37) Ofudje, E. A.; Rajendran, A.; Adeogun, A. I.; Idowu, M. A.; Kareem, S. O.; Pattanayak, D. K. Synthesis of Organic Derived Hydroxyapatite Scaffold from Pig Bone Waste for Tissue Engineering Applications. *Adv. Powder Technol.* **2018**, *29*, 1−8.
(38) Puvvada, N.; Panigrahi, P. K.; Pathak, A. Room Temperature Synthesis of Highly Hemocompatible Hydroxyapatite, Study of Their Physical Properties and Spectroscopic Correlation of Particle Size. *Nanoscale* **2010**, *2*, 2631−2638.
(39) Cestari, F.; Agostinacchio, F.; Galotta, A.; Chemello, G.; Motta, A.; Sglavo, V. M. Nano-Hydroxyapatite Derived from Biogenic and Bioinspired Calcium Carbonates: Synthesis and in Vitro Bioactivity. *Nanomaterials* **2021**, *11*, 264−14.
(40) Lu, H. B.; Campbell, C. T.; Graham, D. J.; Ratner, B. D. Surface Characterization of Hydroxyapatite and Related Calcium Phosphates by XPS and TOF-SIMS. *Anal. Chem.* **2000**, *72*, 2886−2894.
(41) Ishikawa, K.; Ducheyne, P.; Radin, S. Determination of the Ca/P Ratio in Calcium-Deficient Hydroxyapatite Using X-Ray Diffraction Analysis. *J. Mater. Sci. Mater. Med.* **1993**, *4*, 165−168.
(42) Kotula, A. P.; Snyder, C. R.; Migler, K. B. Determining Conformational Order and Crystallinity in Polycaprolactone via Raman Spectroscopy. *Polymer* **2017**, *117*, 1−10.
(43) Baranowska-Korczyc, A.; Warowicka, A.; Jasiurkowska-Delaporte, M.; Grześkowiak, B.; Jarek, M.; Maciejewska, B. M.; Jurga-Stopa, J.; Jurga, S. Antimicrobial electrospun poly(ε-caprolactone) scaffolds for gingival fibroblast growth. *RSC Adv.* **2016**, *6*, 19647−19656.
(44) Timchenko, P. E.; Timchenko, E. V.; Pisareva, E. V.; Vlasov, M. Y.; Volova, L. T.; Frolov, O. O.; Kalimullina, A. R. Experimental Studies of Hydroxyapatite by Raman Spectroscopy. *J. Opt. Technol.* **2018**, *85*, 130.
(45) Buchwald, T.; Kozielski, M.; Szybowicz, M. Determination of Collagen Fibers Arrangement in Bone Tissue by Using Transformations of Raman Spectra Maps. *Spectrosc.* **2012**, *27*, 107−117.
(46) Trakoolwannachai, V.; Kheolamai, P.; Ummartyotin, S. Characterization of Hydroxyapatite from Eggshell Waste and Polycaprolactone (PCL) Composite for Scaffold Material. *Composites, Part B* **2019**, *173*, 106974.
(47) Huang, B.; Caetano, G.; Vyas, C.; Blaker, J.; Diver, C.; Bártolo, P. Polymer-Ceramic Composite Scaffolds: The Effect of Hydroxyapatite and β-tri-Calcium Phosphate. *Mater.*. **2018**, *11* (). DOI: 10.3390/ma11010129.
(48) Jiao, Z.; Luo, B.; Xiang, S.; Ma, H.; Yu, Y.; Yang, W. 3D printing of HA / PCL composite tissue engineering scaffolds. *Adv. Ind. Eng. Polym. Res.* **2019**, *2*, 196−202.
(49) Akhbar, S.; Subuki, I.; Sharudin, R. W.; Ismail, M. H. Performance of Polycaprolactone/Hydroxyapatite (PCL/HA) Composite Blended by Ultrasound Assisted Melt Blending. *J. Mech. Eng.* **2018**, *5*, 235−250.

https://doi.org/10.1021/acsomega.1c05593
ACS Omega 2022, 7, 8323−8335

(50) Taghavi, M. A.; Rabiee, S. M.; Jahanshahi, M.; Nasiri, F. Electrospun Poly-ε-Caprolactone (PCL)/Dicalcium Phosphate Dihydrate (DCPD) Composite Scaffold for Tissue Engineering Application. *Mol. Biotechnol.* **2019**, *61*, 345−354.
(51) Lobo, A. O.; Afewerki, S.; de Paula, M. M. M.; Ghannadian, P.; Marciano, F. R.; Zhang, Y. S.; Webster, T. J.; Khademhosseini, A. Electrospun Nanofiber Blend with Improved Mechanical and Biological Performance. *Int. J. Nanomed.* **2018**, *13*, 7891−7903.
(52) Zhang, Y.; Ouyang, H.; Lim, C. T.; Ramakrishna, S.; Huang, Z.-M. Electrospinning of Gelatin Fibers and Gelatin/PCL Composite Fibrous Scaffolds. *J. Biomed. Mater. Res., Part B* **2005**, *72B*, 156−165.
(53) Croisier, F.; Duwez, A.-S.; Jérôme, C.; Léonard, A. F.; Van Der Werf, K. O.; Dijkstra, P. J.; Bennink, M. L. Mechanical Testing of Electrospun PCL Fibers. *Acta Biomater.* **2012**, *8*, 218−224.
(54) Dwivedi, R.; Kumar, S.; Pandey, R.; Mahajan, A.; Nandana, D.; Katti, D. S.; Mehrotra, D. Polycaprolactone as Biomaterial for Bone Scaffolds: Review of Literature. *J. Oral Biol. Craniofacial Res.* **2020**, *10*, 381−388.
(55) Kim, J.-W.; Shin, K.-H.; Koh, Y.-H.; Hah, M. J.; Moon, J.; Kim, H.-E. Production of Poly(ε-Caprolactone)/Hydroxyapatite Composite Scaffolds with a Tailored Macro/Micro-Porous Structure, High Mechanical Properties, and Excellent Bioactivity. *Mater.* **2017**, *10*, 1123.
(56) Erisken, C.; Kalyon, D. M.; Wang, H. Functionally graded electrospun polycaprolactone and β-tricalcium phosphate nanocomposites for tissue engineering applications. *Biomaterials* **2008**, *29*, 4065−4073.
(57) Yang, F.; Both, S. K.; Yang, X.; Walboomers, X. F.; Jansen, J. A. Development of an Electrospun Nano-Apatite/PCL Composite Membrane for GTR/GBR Application. *Acta Biomater.* **2009**, *5*, 3295−3304.
(58) Apalangya, V. A.; Rangari, V. K.; Tiimob, B. J.; Jeelani, S.; Samuel, T. Eggshell Based Nano-Engineered Hydroxyapatite and Poly(Lactic) Acid Electrospun Fibers as Potential Tissue Scaffold. *Int. J. Biomater.* **2019**, *2019*. DOI: 10.1155/2019/6762575.
(59) Venugopal, J.; Vadgama, P.; Kumar, T. S. S.; Ramakrishna, S. Biocomposite Nanofibres and Osteoblasts for Bone Tissue Engineering. *Nanotechnology* **2007**, *18* (). DOI: 10.1088/0957-4484/18/5/055101.
(60) Shkarina, S.; Shkarin, R.; Weinhardt, V.; Melnik, E.; Vacun, G.; Kluger, P. J.; Loza, K.; Epple, M.; Ivlev, S. I.; Baumbach, T.; Surmeneva, M. A.; Surmenev, R. A. 3D Biodegradable Scaffolds of Polycaprolactone with Silicate-Containing Hydroxyapatite Microparticles for Bone Tissue Engineering: High-Resolution Tomography and in Vitro Study. *Sci. Rep.* **2018**, *8*, 1−13.
(61) Hembrick-Holloman, V.; Samuel, T.; Mohammed, Z.; Jeelani, S.; Rangari, V. K. Ecofriendly Production of Bioactive Tissue Engineering Scaffolds Derived from Egg- And Sea-Shells. *J. Mater. Res. Technol.* **2020**, *9*, 13729−13739.

https://doi.org/10.1021/acsomega.1c05593
ACS Omega 2022, 7, 8323−8335